PM10 Source Apportionment in Five North Western European Cities - Outcome of the Joaquin Project

D. Mooibroek
J. Staelens
R. Cordell
P. Pantelliadis
T. Delauney
E.P. Weijers **(ECN)**
J. Vercauteren
R. Hoogerbrugge
M. Dijkema
Paul S. Monks
E. Roekens

Oktober 2016
ECN-B--15-009

PM_{10} Source Apportionment in Five North Western European Cities—Outcome of the Joaquin Project

DENNIS MOOIBROEK, JEROEN STAELENS,* REBECCA CORDELL, PAVLOS PANTELIADIS, TIPHAINE DELAUNAY, ERNIE WEIJERS, JORDY VERCAUTEREN, RONALD HOOGERBRUGGE, MARIEKE DIJKEMA, PAUL S. MONKS AND EDWARD ROEKENS

ABSTRACT

The aim of this study was to identify and quantify sources contributing to particulate matter (PM_{10}) at four urban background sites and an industrial site in North West Europe using a harmonized approach for aerosol sampling, laboratory analyses and statistical data processing. Filter samples collected every 6th day from April 2013 to May 2014 were analysed for metals, monosaccharide anhydrides, elemental and organic carbon, water-soluble ions and oxidative potential. The receptor-oriented model EPA-PMF 5.0.14 was used to carry out a source apportionment using the pooled data of all sites. A solution with 13 factor profiles was found which could be aggregated into eight groups: secondary aerosol; furnace slacks, road wear and construction; sea spray; mineral dust; biomass burning; industrial activities; traffic emissions and brake wear; and residual oil combustion. The largest part of PM_{10} (40–48%) was explained by nitrate-rich and sulphate-rich secondary aerosol, followed by (aged) sea spray (11–21%). Clear traffic and biomass burning profiles were also found. Conditional probability function plots were used to indicate the likely directions of the sources,

*Corresponding author.

Issues in Environmental Science and Technology No. 42
Airborne Particulate Matter: Sources, Atmospheric Processes and Health
Edited by R.E. Hester, R.M. Harrison and X. Querol

Published by the Royal Society of Chemistry, www.rsc.org

while air mass back-trajectories were analysed using the HYSPLIT model. A better understanding of the composition and sources of particulate matter can facilitate the development of health-relevant air quality policies.

1 Introduction

Northwest Europe is still considered as a hot spot for air pollution with high ambient concentrations of, amongst others, particulate matter (PM) and nitrogen oxides (NO_x).[1] Particulate matter is a heterogeneous mixture of components resulting from multiple natural and anthropogenic sources, including sea salt, naturally suspended dust, pollen, volcanic ash, combustion processes, industrial activities, vehicle tyre and break wear, and road surface wear. Epidemiological studies attribute the most important health impacts of air pollution to PM,[2] although currently it is still unclear which specific properties (such as size and chemical composition) or sources of particles are most relevant to health effects.[3] Ambient PM concentrations vary substantially between and within regions, as indicated for example by routine air quality monitoring networks.[1] In urban areas, in addition to background PM concentrations often imported, traffic-related emissions and domestic heating can significantly contribute to ambient PM levels.[1]

Current monitoring efforts generally focus on the mass concentration of PM_{10} and $PM_{2.5}$ in line with current air quality legislation,[4] but these data generally do not allow the assessment of differing sources. To facilitate the development of health-relevant air quality policies a better understanding of the sources and composition of PM is required. Information about the pollution sources is also required to identify if exceedances are owing to either natural sources (including road salting and sanding) or anthropogenic sources.[4] Using source apportionment additional information can be derived about pollution sources and the amount they contribute to pollution levels.[5] To accomplish this, three main approaches exists: emission inventories, source-oriented models and receptor-oriented models. In this study we have used the receptor-oriented model US-EPA-PMF (Positive Matrix Factorization) to identify and quantify the most relevant sources in NW Europe. The PMF model is based on uncertainty-weighted factor analysis and relies on pollutant measurements. This approach has the advantage of scaling each data point individually using an uncertainty matrix, so that data with a higher precision have a larger influence on the solution.[6]

Information on the composition of PM in NW Europe has been reported before, for example for the north of Belgium,[7] the Netherlands[8] and the United Kingdom,[9] but comparison of the findings between sites or regions is hampered by differences in study periods, analytical methods and modelling and reporting methods. Therefore, the aim of this study was to quantitatively identify sources contributing to PM_{10} at five sites in NW Europe using a harmonized approach for aerosol sampling, laboratory analyses and

statistical data processing. PM_{10} was sampled at four urban background sites and one industrial site and the chemical composition and oxidative potential of PM_{10} were measured. The data of the five sites were pooled to carry out a source apportionment using PMF.

2 Site Description and Chemical Characterisation of PM_{10}

2.1 Sites

Aerosol samples were collected at five sites in NW Europe: Amsterdam (site code: AD), Wijk aan Zee (WZ) (The Netherlands), Antwerp (AP; Belgium), Leicester (LE; United Kingdom) and Lille (LL; France). Table 1 summarizes the characteristics of the sites; detailed site descriptions are given elsewhere.[10] Site WZ is an industrial monitoring site at about 30 km from Amsterdam. The four other sites are considered to be urban background sites for PM_{10} monitoring, although there is considerable influence of local traffic. Traffic data for AD,[11] LE[12] (2013) and AP[13] (February and October 2013) show that traffic intensity was highest near AP, which was also closest to a main road. Air quality monitoring at AD, AP and LE indicated a clear traffic-related diurnal variation in black carbon and ultrafine particles at these sites.[10]

Table 1 Location and characteristics of the five PM_{10} sampling sites (traffic intensity data for 2013).

City	Code	Latitude	Longitude	Description
Amsterdam	AD	52°21′35″ N	4°51′59″ E	Near Vondelpark, 64 m south from a main road (Overtoom, 15 000 vehicles day^{-1}).
Antwerp	AP	51°12′35″ N	4°25′55″ E	In Borgerhout, 30 m north from of a main road (Plantin en Moretuslei, 29 500 vehicles day^{-1}).
Leicester	LE	52°37′12″ N	1°07′38″ W	At the main campus of the University of Leicester, 140 m northeast from a main road (Welford Road, 22 500 vehicles day^{-1}).
Lille	LL	50°37′41″ N	3°05′25″ E	At a school campus in Lille Fives, 35 m north from a local road (rue du Vieux Moulin, no traffic data available).
Wijk aan Zee	WZ	52°49′40″ N	4°60′23″ E	On a parking lot, 70 m north from a local road (Burgemeester Rothestraat, no traffic data available).

Wind speed and direction were recorded at meteorological monitoring stations located at a distance of 3–7 km from the aerosol sampling sites (AD: Schiphol airport, AD: Antwerp Luchtbal, LE: Groby Road, LL: Sequedin, WZ: IJmuiden), as detailed elsewhere.[10] As the wind was not measured at the receptor sites, the available data can be considered to be representative for regional wind conditions but do not account for the potential influence of *e.g.* high buildings on wind conditions in urban environments.

2.2 PM_{10} Sampling and Gravimetric Analysis

Sampling was carried out for 14 months (426 days) from 1 April 2013 to 31 May 2014, except for LL where the measurements started 2 months later (5 June 2013 to 31 May 2014). The samples were collected daily (24 hour exposure) onto 47 mm quartz filters (Pall Tissuquartz™ filters, 2500 QAT-UP) using a sequential sampler (Derenda PNS16 at AD and WZ and Leckel SEQ47/50 at AP, LE and LL) with a PM_{10} inlet running at 2.3 m^3 h^{-1} for 24 h per filter. Flows were checked every 14 days when changing the filter compartments. Filters were weighed before and after sampling in order to determine total PM_{10} mass according to the (stricter) standard for $PM_{2.5}$.[14] Before and after sampling, filters were conditioned at 20 ± 1 °C and $50 \pm 5\%$ relative humidity for 48 h, weighed, left for a further 24 h and re-weighed. After gravimetric analysis, filters were stored at −18 °C. Ambient nitrogen oxide concentrations were measured continuously at the five sites by chemiluminescence NO-NO_2-NO_x analysers (API 200A at AD and WZ and Thermo 42i at AP, LE and LL).

2.3 Chemical Analysis

One in six filters was used for chemical analysis. Six punches of 1×1 cm^2 (puncher manufactured by Sunset Laboratory Inc., USA) were taken per filter and transported in cooling boxes to the different laboratories. Three punches were analysed for metals, monosaccharide anhydrides (MAs) and elemental and organic carbon (EC and OC), respectively. The other three punches were used to determine water-soluble ions and the remaining filter part was analysed for oxidative potential (OP). Each type of analysis was carried out by a single laboratory for all the samples. After microwave-assisted acid digestion (HNO_3/H_2O_2), calcium (Ca), iron (Fe), potassium (K) and zinc (Zn) were quantified by inductively coupled plasma optical emission spectroscopy (ICP-OES) and aluminium (Al), titanium (Ti), vanadium (V), chromium (Cr), manganese (Mn), nickel (Ni), copper (Cu), arsenic (As), molybdenum (Mo), cadmium (Cd), antimony (Sb), barium (Ba) and lead (Pb) by inductively coupled plasma mass spectrometry (ICP-MS). The HNO_3/H_2O_2 digestion leads to incomplete recovery of Al and Ti because HF is needed to dissolve aluminium silicates, but was chosen because it results in a lower limit of detection (LOD) for most elements. The MAs levoglucosan, mannosan and galactosan were quantified using a validated gas chromatography

mass spectrometry (GC-MS) method described in detail previously.[15] The EC/OC content was analysed according to CEN/TR 16243[16] using a laboratory organic/elemental carbon aerosol analyser (Sunset Laboratory Inc., USA) and the NIOSH protocol, which was considered to be most suitable for the traffic-influenced PM_{10} samples in this study. The water-soluble ions were determined according to CEN/TR 16269.[17] After ultrasonic water extraction, potassium (K^+), calcium (Ca^{2+}), magnesium (Mg^{2+}) and sodium (Na^+) were analysed by ICP-OES and ammonium (NH_4^+), chloride (Cl^-), nitrate (NO_3^-) and sulfate (SO_4^{2-}) by ion chromatography with conductivity detection (IC-CD). The method used for the detection of the oxidant (radical) generation capacity of PM was electron paramagnetic resonance (EPR) spectroscopy using the spin trap 5,5-dimethyl-1-pyrroline-*N*-oxide (DMPO). The OP was determined directly on the filter material without prior PM extraction.[18]

In addition to the filters collected every 6th day from April 2013 to May 2014, the analyses were also carried out for 6–9 filters taken every 2nd day for three sites (AD: $n = 6$ in April 2013; AP: $n = 8$ in September 2013; LE: $n = 9$ in March 2014) and for 17 filters per site taken on days with regionally enhanced PM_{10} levels (10 April and 25 September 2013; 30 January, 5–15 March, 30 March to 3 April, and 24 April 2014). Over the study period 68 field blank filters, which were kept in the sampling devices for 14 days without exposure to sampled air, were also analysed as part of the quality control.

3 Source Apportionment Using Positive Matrix Factorization

3.1 Data Preparation and Uncertainty Matrix

For the five sites, in total 434 valid filters were available for the source apportionment analysis ($n = 94$ for AD, 95 for AP, 89 for LE, 72 for LL and 84 for WZ). In addition, the analysis included 31 filters that were collected during short sampling campaigns using a mobile trailer (Leckel SEQ47/50) at a second urban background site in Amsterdam (6 km from AD, May 2013, $n = 8$), Antwerp (1 km from AP, Oct 2013, $n = 12$) and Leicester (1 km from LE, April 2014, $n = 11$).[19] These filters were analysed as described above. In the present study we focus on the five main sites (Table 1) because at the three temporary sites only a few samples were collected with a PM_{10} composition that was generally similar to those of the main site nearby (AD, AP, LE).

Ambient concentrations of the measured variables per filter were calculated based on the exposed surface area of the filter, which was considered to be a constant value per sampling device, and the sampled air volume measured per sampling device and day. No correction was carried out for the concentrations of blank filters. The amount of missing chemical data was generally negligible, except for Al, Ca, Ti and Zn. Owing to sample contamination in the laboratory, results of these elements were lacking for 171 filters (39%). The missing data were estimated by multiple imputation,[20] a technique frequently applied in environmental research and biostatistics.[21,22]

Some variables have less additional informative value in the PMF analysis and are therefore downscaled or excluded. In this study the following classification was used: (1) the PM_{10} mass from the weighed filters was included as default mass variable and hence automatically downscaled; (2) Al, Ca, Ti and Zn were downscaled owing to the large number of missing values; (3) total K was excluded because the concentrations were often lower than for the water-soluble fraction K^+, likely owing to the low levels of ambient K and K^+ compared to the LOD of the analytical methods; and (4) OP, NO and NO_2 were downscaled because in the present study they were not considered as driving variables, however the distribution of their concentrations in the profiles is of interest, *e.g.* to test the validity of a traffic profile. This resulted in a data set of 465 samples with 33 variables, including PM_{10} mass, 25 of which were categorized as strong.

The coefficient of variation (CV) and LOD of each variable were estimated based on the relative standard deviation of repeated analyses of blanks and exposed filters. The CVs and LODs were used to calculate the uncertainties (unc) for a given concentration level (conc) with the following equation:

$$\text{unc} = \sqrt{(0.5 \cdot \text{LOD})^2 + (\text{CV} \cdot \text{conc})^2} \quad (1)$$

Chemical results below LODs were not replaced by a fixed value. However, uncertainties for values below the LOD were set equal to the LOD. For imputed values the uncertainties were increased by a factor of four. This ensured that imputed values and values below the LOD had less weight in obtaining the final solution.

3.2 Positive Matrix Factorization

The source apportionment was carried out with US-EPA-PMF 5.0.14, a programme that uses ME-2 as the underlying engine to solve the PMF problem.[23,24] The calculations were performed in robust mode, in which outliers have less influence on the obtained solution. The data of all sites were pooled prior to the PMF analysis. This approach increases the size of the data set and hence decreases the significance of random errors and errors owing to rotational ambiguity.[25] However, this approach assumes that there is little variance between the composition of the source profiles between the sites. In other words, the main variability is assumed to be found in the contribution of each factor at the different sites.

When applying the PMF technique, the number of factors has to be selected. An indicator for selecting this number is the ratio between the (robustly) calculated and expected values of the sum-of-squares object function (Q) that is minimized in the PMF. Runs were carried out with 2 to 20 factors to evaluate the robust to expected Q value (Q ratio) and to examine the composition of the obtained factors. A solution with 13 factor profiles was selected because this yielded the most physically interpretable results. The Q ratio for this solution was approximately 6, which is larger than the

expected ratio of 1. Part of this increase can be explained by the decision to pool the data from all receptor sites, as multiple-site data will have a higher Q ratio owing to the variation in source composition between the sites. Brown *et al.*[26] reported Q ratios between 2 to 5.5 for single-site data, which is fairly similar to the Q ratio in the present study. Furthermore, even while performing calculations in robust mode, it might be difficult to assess if the calculated Q value is as expected or too large. In this case, it might be helpful to examine the scaled residuals, *i.e.* the residuals divided by their error estimates. In a well-fit model these scaled residuals should be symmetrically distributed and lie in the -3 to $+3$ range. The majority of all scaled residuals were generally within this range, except for K^+, Ba, Fe, Mo, Ni, Sb and the MAs, for which the distribution of the scaled residuals was skewed to the right. This may be owing to high concentrations at one or two sites, probably by extending the data set of the predefined filter samples taken every 6th day with the samples on days with enhanced PM_{10} values. To examine the effect of the uncertainties an indicative analysis was performed, with 13 factors and an 'added modelling uncertainty' of 15%. This decreased the Q values and made the Q ratio approach unity, but only had a small influence on the composition of the resulting factors. It was therefore decided to evaluate the 13 factor solution without added modelling uncertainty.

Even though a global minimum of the Q function is found by the least squares fitting process, there may not be a unique solution because of rotational ambiguity. The addition of constraints such as non-negativity can reduce the rotational freedom in the model, but non-negativity alone does not generally produce a unique solution.[27] The PMF algorithm provides a 'peaking parameter' called FPEAK allowing the user some control over the rotations. If a value of zero is used for this parameter, the algorithm will produce a more central solution. The use of non-zero values allows sharper peaks to be obtained, which are to be expected in source profiles, and will limit the rotational freedom.[6,28] Several runs with different positive and negative FPEAK values were performed to get more insight into the rotational freedom of the solution. Judging from the change in Q values, there was not much improvement over the 'central' solution (FPEAK $= 0$), which consequently has been used in the rest of this study.

The degree of spatial uniformity of the calculated source contributions between the receptor sites was determined using the coefficient of divergence (COD).[22,29] If the source contributions are similar at all sites, the COD approaches zero. In case the source contributions are very different, *e.g.* highly impacted by local sources, the COD approaches unity.

Conditional probability function (CPF) plots were used to indicate directions in which sources are likely to be located.[22,30] The CPF was calculated using the upper 25th percentile of the source contributions from the PMF analysis and the wind direction values measured on meteorological stations near the sites. To match the hourly wind data, each daily contribution was assigned to each hour of a given day.[31] Back-trajectories of air masses during specific periods were analysed using the Hybrid Single-Particle Lagrangian

Integrated Trajectory (HYSPLIT) model.[32] By performing a backwards trajectory the model follows a single air parcel backwards in time, providing information about the origin of a local or regional source. For the interpretation of the CPF plots, it should be noted that the wind data used are representative for area sources but might be less representative for local sources in urban areas (*e.g.* traffic) because of the potential influence of high buildings on wind speed and direction. For trajectory analyses, however, regional meteorology is most relevant.

The European air quality directive[4] has set two limit values for PM_{10}, one of which is that the daily mean PM_{10} value may not exceed 50 μg m^{-3} more than 35 days in a year. The contribution matrix calculated by PMF contains factor contributions for each sample day included in the analysis. We have selected the days with known PM_{10} composition on which the PM_{10} concentration was above 50 μg m^{-3} to determine the contribution of the calculated sources on these exceedance days.

The PMF model version used contains three methods for estimating the uncertainty in a PMF analysis owing to random errors and rotational ambiguity: classical bootstrap (BS), displacement of factor elements (DISP), and bootstrap enhanced by displacement of factor elements (BS-DISP). The three methods are considered complementary; depending on the situation one method might provide better results than the other methods.[25] Therefore, the uncertainty of the 13-factor solution was analysed according to the three methods. In our evaluation NO_3^-, Cl^-, SO_4^{2-}, Na^+, NH_4^+, Ca^{2+}, Cr, Cu, Fe, Mn, Pb, V, levoglucosan and EC were included as 'key species' for the BS-DISP method. A general problem in comparing uncertainty analysis results is that species concentrations differ in magnitude. In our study this is for example evident by including the OP of PM_{10}, with much higher values compared to other species. To compare the results among species, the so-called interval ratios of the BS, DISP and BS-DISP methods were used.[25,26]

4 Results and Discussion

4.1 PM_{10} Mass Concentrations

During the common sampling period at the five sites (1 June 2013 to 31 May 2014), the mean PM_{10} concentration was highest at the site in Wijk aan Zee (WZ; annual mean of 25.0 μg m^{-3}) and Antwerp (AP; 24.5 μg m^{-3}), intermediate in Lille (LL; 22.4 μg m^{-3}) and Amsterdam (AD; 20.3 μg m^{-3}) and lowest in Leicester (LE; 16.0 μg m^{-3}). Data coverage during this period was 90–97% depending on the site. The number of exceedances of the EU day limit value[4] for PM_{10} (50 μg m^{-3}) was highest at AP (20 days $year^{-1}$) and WZ (16), moderate at LL (12) and lowest at AD (8) and LL (6). Exceedances of the day limit value mainly occurred in March and April. Sampling started 2 months earlier at all sites other than LL, and the mean PM_{10} values for this 14 month period (Figure 1, left boxplot for each site) differed by less than 2% from the annual means.

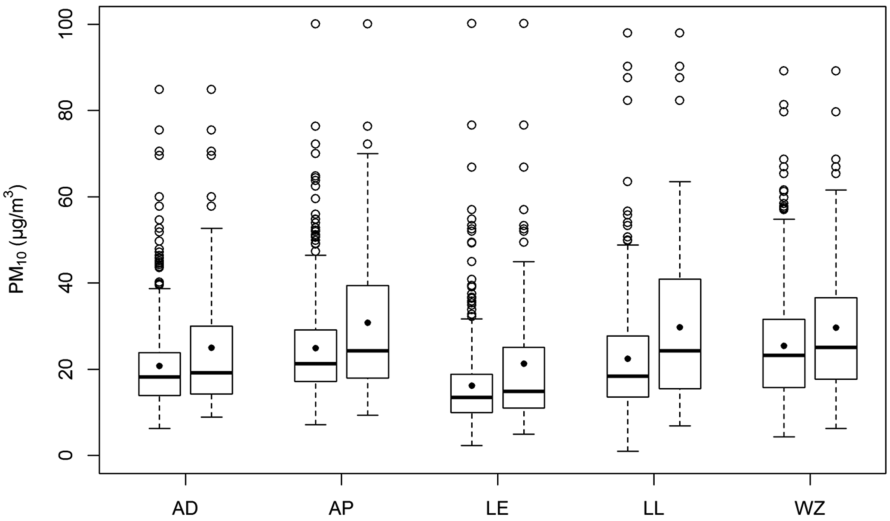

Figure 1 Boxplots of daily PM_{10} (µg m^{-3}) at the five sites (see Table 1) according to all valid filters (left boxplot per site) and according to the filters used for source apportionment (right boxplot per site) (dot: mean value; line in box: median value; box: 25th and 75th percentiles; whiskers: 1.5 times the interquartile range from the box).

In this study a subset of daily filters was selected for chemical analyses and source apportionment, so it is relevant to evaluate the representativeness of the selected days. The data set mainly consisted of filters collected every 6th day; the mean PM_{10} concentration for these data differed less than 2% from the 12/14 month mean per site. By expanding the data set with 6–9 filters per site taken every 2nd day and with 17 filters per site for days with regionally enhanced PM_{10} levels, the PM_{10} distribution per site was shifted upwards (Figure 1, right boxplot per site). Figure 2 presents the time variation of PM_{10} per site for the source apportionment data used in this study. The relative similarity across the five sites over time indicates a regional pattern of PM_{10}. A detailed description of all the measurement results, including time series and site comparisons per individual PM_{10} composition variable, is reported elsewhere.[19]

4.2 Identification and Temporal Variation of the Calculated Factors

Figure 3 shows the normalized factor profiles, indicating the fraction of all the measured variables accounted for by each factor. The chemical fingerprint of factor 1 consists primarily of markers associated with nitrate-rich secondary inorganic aerosols (NO_3^- and NH_4^+). Based on the calculated contributions of this profile we observed a seasonal pattern (results not shown) consisting of higher concentrations during the autumn/winter

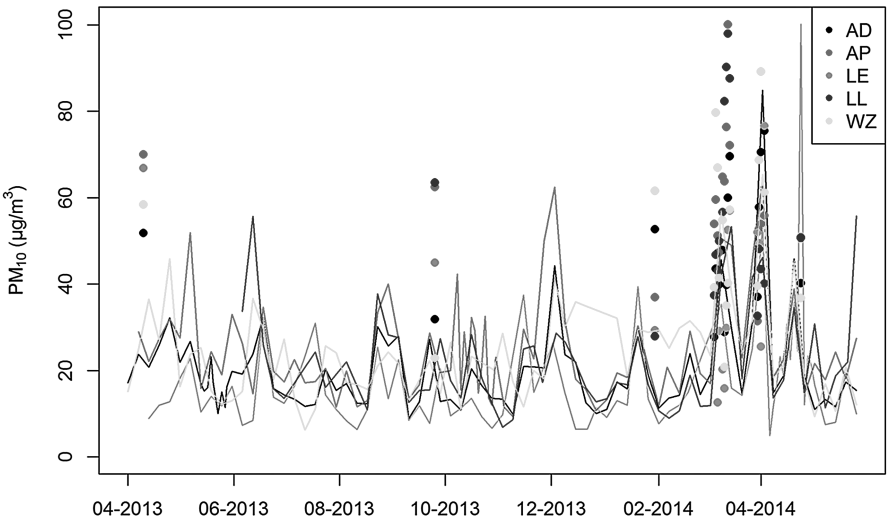

Figure 2 Time variation of daily PM_{10} (µg m^{-3}) at the five sites according to the filters used for source apportionment. Full lines present data of the 1 in 6th day and 1 in 2nd day filters, dots show the additionally analysed filters for days with regionally enhanced PM_{10} ($n = 17$ per site).

period compared to the summer/spring period. It is well known that temperature greatly affects the equilibrium of ammonium nitrate (NH_4NO_3), ammonia (NH_3) and nitric acid. Low temperature during the autumn/winter period favours the formation of the particulate form.[22] Nitrate is formed by the oxidation of NO_2 emitted by combustion processes, such as vehicle engines. This process is slow, which explains the small contribution of NO_2 and other combustion indicators associated with this factor. Nevertheless, a limited contribution of OC is found in this factor. This observation is however not unrealistic because part of the OC is also thought to be semi-volatile.[33] Similar results have been reported for the Netherlands.[34,35] We categorized factor 1 as 'nitrate-rich secondary aerosol (SA)'. Factor 2 mainly contains secondary sulfate, as indicated by the presence of SO_4^{2-} and NH_4^+, and a limited contribution of OC. Secondary sulfate is formed from atmospheric oxidation of SO_2 and is associated with long-range transport. It exhibits a seasonal variation with higher contributions during the summer period.[22] Factor 2 is categorized as 'sulfate-rich SA'.

Factor 3 contains the majority of the Ca contributions. In general, Ca is commonly associated with mineral dust, building activities and fertilizers. However, Ca has also been related to vehicular emissions and iron and steel plants.[36–38] Iron and steel plants commonly produce furnace slacks, *i.e.* the glass-like by-product left over after a desired metal has been separated (*i.e.*, smelted) from its raw ore. It consists mainly of Ca, silicon (Si), Mg, and Al oxides. Furnace slacks are commonly used in asphalt which is a composite material used to surface roads, parking lots and airports. Additionally,

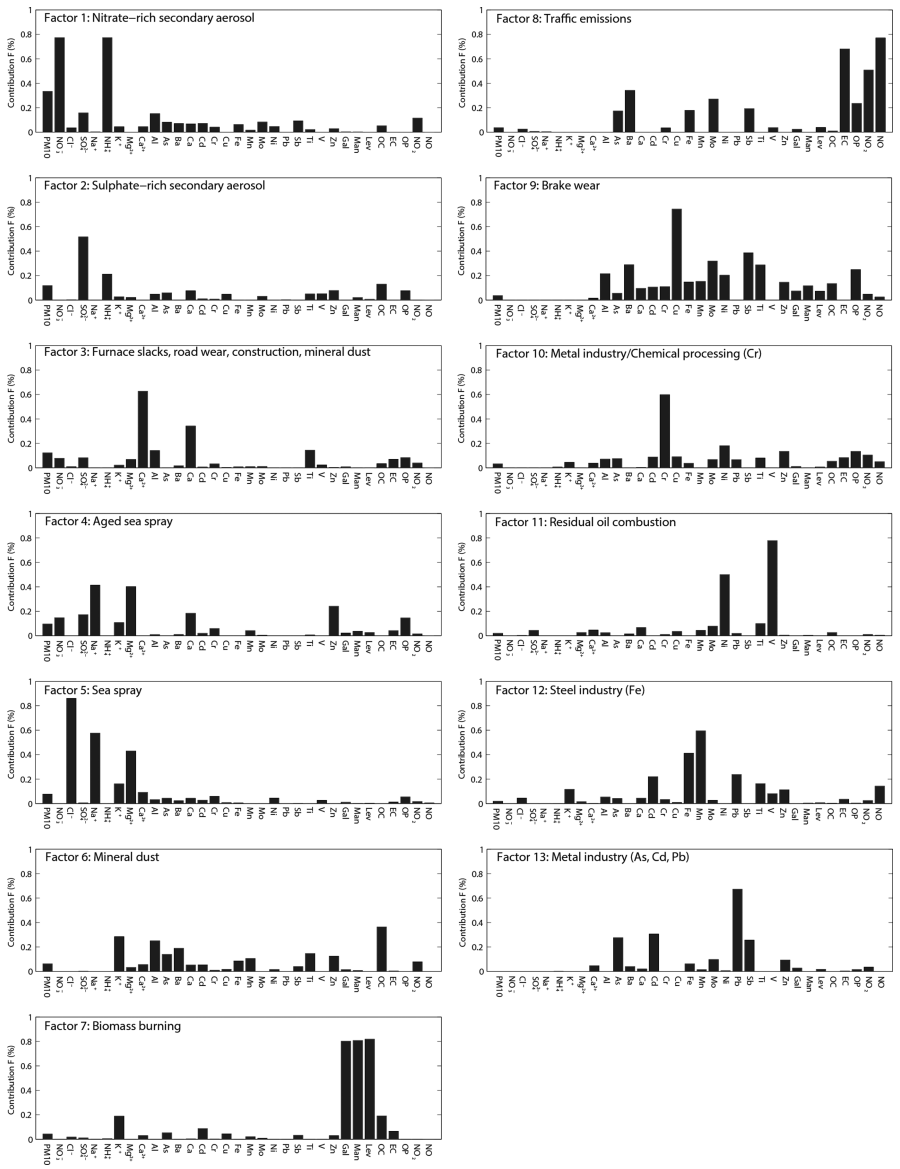

Figure 3 Normalized US-EPA-PMF source profiles based on the chemical composition, the oxidative potential (OP) of PM_{10} and the ambient NO and NO_2 concentration (average profiles for the five sites).

building/concrete debris is also used as the mineral aggregate in asphalt. In another source apportionment study in Amsterdam[39] a crustal component based on a high loading of Ca was found. Despite the large contribution of Ca in that study[39] no other typical crustal elements, such as Al and Ti, were detected, and the profile was not associated with any wind direction,

suggesting it was not emitted by a single major point source in or near Amsterdam. Valius[39] associated this profile to a distinctive composition profile of the resuspended road dust near the measurement site. The different composition profile was thought to be a consequence of the widespread use of road structures made from asphalt/concrete in Amsterdam. In the present study, contributions of factor 3 are found at all sites, with WZ and AP showing the highest contributions. The high contributions found at WZ might be primarily associated with the storage/transhipment of furnace slacks from the nearby steel melting furnace. However, this does not explain the high contributions at AP. Compared to the other sites, AP is most closely located to a main road with high traffic intensity, so part of the contributions may be caused by the wear and tear on the asphalt/concrete roads owing to traffic. However, factor 3 does not show a seasonal variation associated with traffic emissions so not all contributions can be related to road surface wear. It is plausible that part of the contribution of this factor is associated with mineral dust and construction/building. Factor 3 is categorized as 'furnace slacks, road wear, construction, mineral dust'.

Factor 4 is characterized by high amounts of Na^+, Mg^{2+} and some SO_4^{2-}. Both Na^+ and Mg^{2+} are associated with sea spray. The factor does not contain Cl^-, which can be explained by chloride depletion, commonly seen in aged sea spray.[40,41] This depletion is directly correlated with the retention time. During this time chloride can be removed from sea salt particles in the air when it reacts to HNO_3 as well as H_2SO_4. In both cases Cl^- becomes associated with the gaseous HCl. The amount of (secondary) NO_3^- and SO_4^{2-} associated with this profile suggest a longer retention time than fresh sea spray. Factor 4 is categorized as 'aged sea spray'. In factor 5 the majority of Na^+, Mg^{2+} and Cl^- concentrations were found, which are associated with sea salt particles. Traces of K^+ and Ca^{2+} are also associated with these particles. The lack of NO_3^- and SO_4^{2-} in this factor suggests a short retention time in the air. This is supported by the high amount of Cl^-, showing limited signs of Cl^- depletion. The Cl^-/Na^+ ratio in this profile is 1.8, corresponding with that found in an earlier study.[22]

Factor 6 is identified by the presence of Al, Ti, Fe and Ca, species that are all associated with mineral dust. This factor also contains a significant portion of OC, which is an indication of mixing of dust and organic matter contributed by biogenic sources (*e.g.* plant detritus or other plant fragments) during resuspension.[41–43] The profile also contains a high amount of K, which can be attributed to sources like mineral dust, combustion and industrial activities. For WZ and AD high source contributions were found at Easter in 2014 (20 April). Factor 6 is categorized as 'mineral dust'. Factor 7 contains almost all available concentrations for the MAs, which are considered to be biomarkers for biomass or wood burning. A small amount of K^+ is also found in this factor and is commonly associated with biomass burning.[44] The factor shows some OC, but the attributed concentration is smaller than the sum of the apportioned MA concentrations. Since the MAs are part of the OC fraction, this indicates that not enough OC is apportioned

to this profile. The highest amounts of biomass burning are found at LL, initially showing a seasonal pattern with high contributions during wintertime. Both AD and WZ show distinct peaks on 30 January and 20 April 2014. The latter is associated with bonfires during Easter commonly seen in the east of the Netherlands as well as Germany. As mentioned, factor 6 (mineral dust) contains high amounts of OC and K^+ and also has a high peak during Easter. Therefore, part of the OC and K^+ in factor 6 is likely related to biomass burning.

Factor 8 contains high amounts of EC, NO_2 and NO, which are commonly associated with primary traffic emissions. In this factor, these species represent the tail-pipe emissions. To a lesser extent, this profile also contains Ba, Mo and Sb. Barium emissions are linked to tyre wear[45] whereas Mo is used as an additive to lubricants and is also released by the combustion of fossil fuels.[46] The highest contribution of this profile is found at AP, which is a traffic-exposed background site. A clear weekend/weekday variation for this profile is found as well as increased contributions during autumn and winter. Factor 8 is categorized as 'traffic emissions'.

Factor 9 is associated with a range of metals (Fe, Cu, Ba, Mn, Mo and Sb) and some OC. The presence of high amounts of Cu along with these other metals suggests this factor is mostly associated with brake wear emissions.[22,47] As this factor is coupled with Al and some Ca and Ti, this would suggest resuspension of traffic-related crustal material. Similar to the traffic emissions a clear weekend/weekday variation for this profile is found at AP as well as increased contributions during autumn and winter. Factor 9 is categorized as 'brake wear'. High contributions of Cr in factor 10 are found at AD, AP and WZ, in contrast to the low contributions at LE and LL. Chromium is associated with several sources, such as traffic and industrial activities. The lack of other markers for traffic or industry hampers the identification of factor 10, which is dubbed as 'metal industry/chemical processing (Cr)'.

In factor 11 significant fractions of Ni and V are found, which are known tracers for the combustion of crude oil.[48] Typical oil combustion sources are shipping,[49] municipal district heating power plants and industrial power plants using heavy oil.[22] While the profile does contain the majority of V, it contains only about 30% of the Ni concentration, suggesting there is at least one other Ni source. Factor 11 is called 'residual oil combustion'. Factor 12 is characterized by high amounts of Fe, Mn and Cd, species commonly associated with the steel industry. The contributions are high at WZ, a site impacted by the presence of a steel industry nearby. We dubbed this profile as 'steel industry (Fe)'. Factor 13 contains high contributions of As, Cd and Pb, which are commonly associated with the metal industry, but are also related to other sources. An example is the bioaccumulation of metals in plants, which are released in the atmosphere by biomass burning. Factor 13 is categorized as 'metal industry (As, Cd, Pb)'. In this analysis no PM_{10} mass was apportioned to the profile metal industry (As, Cd, Pb), despite the distinct chemical fingerprint. This occasionally happens when there is some

Table 2 Linear regressions and coefficient of determination (R^2) between the measured and predicted (apportioned) PM_{10} mass per site.

Site	Linear regression equation	R^2
AD	Predicted mass = 0.37 + 0.98 · total mass	0.98
AP	Predicted mass = 0.71 + 0.98 · total mass	0.98
LE	Predicted mass = 2.94 + 0.84 · total mass	0.81
LL	Predicted mass = 1.70 + 0.94 · total mass	0.94
WZ	Predicted mass = 0.29 + 0.99 · total mass	0.98
Full data set	Predicted mass = 2.01 + 0.92 · total mass	0.91

rotational ambiguity in the solution as well as very low PM_{10} concentrations with high uncertainties associated with this source.

Table 2 shows the relationships between the measured and apportioned PM_{10} mass per site and for the full data set. The lowest coefficient of determination was found for LE ($R^2 = 0.81$), suggesting that the current suite of profiles and corresponding contributions are not an optimum match for the actual situation at LE.

4.3 Spatial Variation of the Source Profiles

Figure 4 shows the relative source profile contributions per sampling site as a percentage of the total PM_{10} mass concentration. The 13 profiles in Figure 4 have been aggregated to eight groups plus an unexplained fraction. The unexplained fraction is defined as the difference between the sum of the mean apportioned and measured PM_{10} mass concentration at each site. Table 3 compares the individual source profiles between the sites, expressed in mass concentration units ($\mu g\ m^{-3}$). The largest part of PM_{10} (40–48%) was explained by SA, which was mainly owing to the nitrate-rich SA factor. The two SA profiles were estimated to contribute similar mass concentrations at the four sites on the European continent (12–13 $\mu g\ m^{-3}$), but had clearly lower values at the UK site LE (8.4 $\mu g\ m^{-3}$). Nitrate-rich SA accounted for 27% (LE) to 37% (LL) of the PM_{10}, while sulfate-rich SA contributed 9–13%. The high contribution of nitrate-rich SA, with NH_4NO_3 as main compound, indicates that decreasing the emissions of its precursor gases NO_x and NH_3 can meaningfully reduce the PM concentrations. For example, a model study found that a reduction of NH_3 emissions by 50% could lead to a 24% reduction of the $PM_{2.5}$ concentrations in NW Europe, mainly driven by reduced formation of NH_4NO_3.[50]

The second-most important source profiles were related to sea spray (11–21% of PM_{10}). The fresh and aged sea spray profiles contributed most PM_{10} in absolute term at WZ (6.3 $\mu g\ m^{-3}$ or 21%), which is the site closest to the North Sea. The absolute contribution was lower and similar at the other four sites (3–4 $\mu g\ m^{-3}$), even though at AD and LE sea spray was relatively more important (17–20%) than at AP and LL (11–13%) because of the lower total PM_{10} levels at AD and LE. The source profile furnace slacks, road wear and construction was on average the third most important, but there was

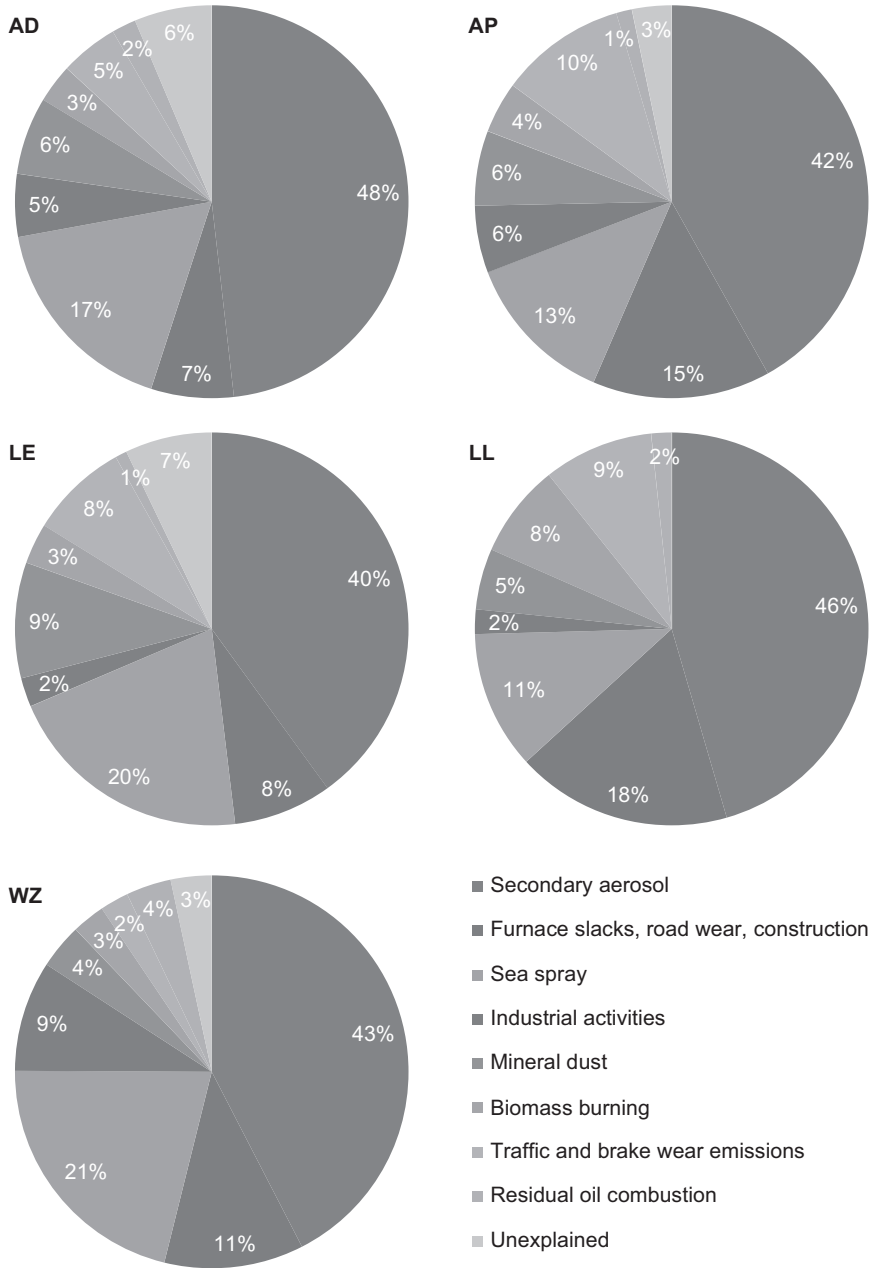

Figure 4 Source contributions (% of the apportioned PM_{10} concentration per site) per site.

more variation between the receptor sites both in the absolute as well at the relative contributions. The estimated mass contribution of furnace slacks, road wear and construction was lower at AD and LE (1.7 μg m^{-3} or 7–8%)

Table 3 Contribution of source profiles (μg m^{-3}) to the measured PM_{10} per site.

	Contribution to PM_{10} (μg m^{-3})				
Source profile	AD	AP	LE	LL	WZ
Secondary aerosol	12.1	12.9	8.4	13.6	12.6
Nitrate-rich secondary aerosol	9.1	9.9	5.8	10.9	8.8
Sulfate-rich secondary aerosol	3.0	3.0	2.6	2.7	3.8
Furnace slacks, road wear, construction	1.7	4.5	1.7	5.3	3.4
Sea spray	4.3	3.9	4.3	3.4	6.3
Aged sea spray	2.5	2.5	2.4	1.9	2.8
Sea spray	1.8	1.4	2.0	1.5	3.4
Mineral dust	1.6	1.9	2.0	1.5	1.1
Biomass burning	0.8	1.3	0.7	2.3	0.8
Industrial activities	1.3	1.7	0.5	0.6	2.7
Metal industry/chemical processing (Cr)	1.1	1.3	0.4	0.4	1.1
Steel industry (Fe)	0.2	0.4	0.2	0.2	1.6
Metal industry (As, Cd, Pb)	0.0	0.0	0.0	0.0	0.0
Traffic emissions and brake wear	1.2	3.2	1.7	2.7	0.7
Traffic emissions	0.5	1.6	0.9	1.2	0.5
Brake wear	0.7	1.5	0.8	1.5	0.2
Residual oil combustion	0.5	0.4	0.2	0.5	1.1
Unexplained	1.6	1.0	1.5	0.0	1.0
Total measured PM_{10}	25.0	30.8	21.1	29.8	29.6

than at WZ (3.4 μg m^{-3} or 11%) and highest at AP and LL (4.5–5.3 μg m^{-3} or 15–18%).

The three source profiles for industrial activities were most important at AD and AP, and in particular at WZ. Metal industry/chemical processing (Cr) was estimated to contribute similarly at these three sites (1 μg m^{-3} or 4%), with lower levels at LE and LL, suggesting that this source had a minor impact on PM_{10} concentrations at LE and LL. The steel industry (Fe) profile was only important at WZ (1.6 μg m^{-3} or 5%). As mentioned earlier, the PMF analysis did not apportion any PM_{10} mass to the metal industry (As, Cd, Pb) profile. However, the PMF output also provides a scaled contribution matrix, which revealed that the largest scaled contribution for the metal industry (As, Cd, Pb) profile was at the receptor site in Antwerp. This indicates the physical relevance of this profile, because upwind of AP (255–225 °N) an industrial site is located that is known to emit As, Cd and Pb.

The biomass burning profile was higher at LL (2.3 μg m^{-3}) and AP (1.3 μg m^{-3}) than at the other sites (0.7–0.8 μg m^{-3}). The mineral dust profile contributed on average 1.1 (WZ) to 2.0 μg m^{-3} (LE), in agreement with the value of 2 μg m^{-3} reported for the regional mineral contribution to total PM_{10} in most of Northern and Central Europe.[51]

The contribution by traffic-related emissions was split up over different source profiles. The PMF analysis resulted in two distinct traffic-related profiles: primary traffic emissions (exhaust) and brake wear, which were highest at LL (2.7 μg m^{-3}) and AP (3.2 μg m^{-3}). For AP this seems logical

since the sampling site has the closest distance to a main road with high traffic intensity. The high contribution of brake wear at LL is somewhat conspicuous as there are no traffic lights near the site. However, a shunting site for trains is located near the site. Shunting in general requires some stop and go actions from trains, so part of the brake wear at LL might be associated with this activity.

In addition to traffic emissions and brake wear, other profiles in this study also contribute to traffic-related PM_{10}, *e.g.* the secondary nitrate-rich SA profile, the furnace slacks, road wear and construction profile and the mineral dust profile. Hence, the sum of the traffic emissions and brake wear profiles in the current study underestimates the actual contribution of road traffic to ambient PM_{10}. For example, for five cities in Flanders the annual PM_{10} concentration in 2013–2014 was on average 7 $\mu g\ m^{-3}$ (or 38%) higher in busy street canyons than at a background location near the city.[52] This local contribution was mostly owing to two approximately equally important traffic-related contributions: the contribution of EC and organic matter in exhaust gases on the one hand and the contribution of mineral dust by soil dust resuspension and the wear of vehicles (tires, brakes, bodywork) and the road surface on the other hand.[52]

The spatial variation between the sites was also evaluated using the COD values per source profile (Figure 5). We found that the steel industry (Fe) profile had the largest COD, indicating very different source contributions between the sites. The highest contributions for the steel industry profile

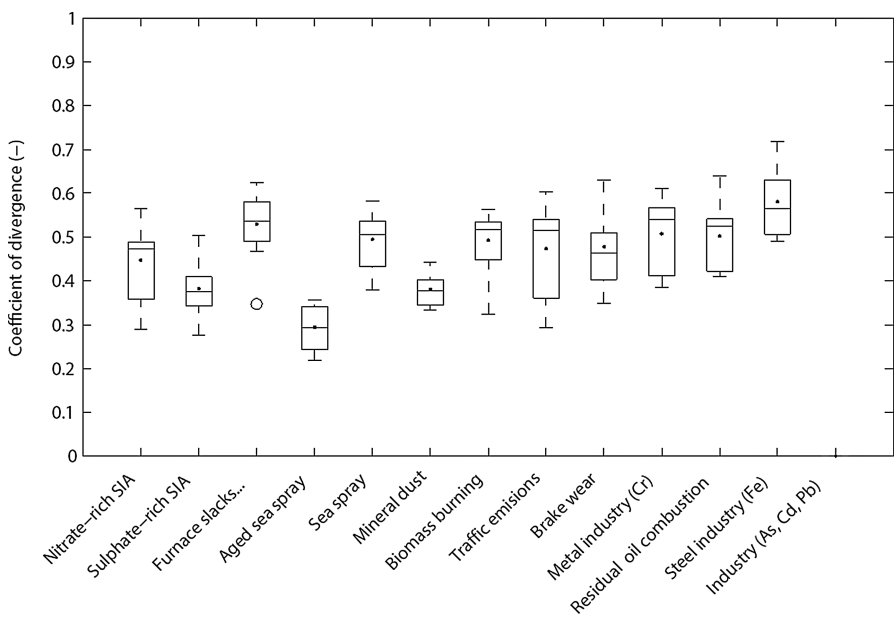

Figure 5 Coefficient of divergence between the five sampling sites per PM_{10} source profile (for explanation of boxplots see Figure 1).

were found at WZ, which is directly impacted by steel industry located south of the receptor site. The factor with the lowest spatial variability was aged sea spray, closely followed by sulfate-rich SA. The small spatial variation reflects the importance of long-range transport into and across the monitored area.[22] Smaller CODs for sulfate-rich SA compared to the nitrate-rich SA have been reported.[53] In the present study the nitrate-rich SA contribution at LE is considerably smaller than at the other sites, indicating a difference in precursor concentrations.

The largest CODs for the traffic emissions profile were found between WZ and the four other sites. This indicates that the contribution from this source is primarily local in the urban environment and the spatial variability is very similar across urban sites in NW Europe. Interestingly, the brake wear source showed a similar behaviour. However, the spatial variability for brake wear between the sites other than WZ was larger compared to traffic emissions. The reason may be that AP, LE and LL are impacted from nearby traffic junctions, leading to a higher contribution of brake-related emissions. Aged sea spray showed the smallest COD values, indicating that this can be considered as an area source. The fresh sea spray profile had larger CODs; the largest contribution of this profile was found at locations relatively close to the sea. The CODs for mineral dust were lower than for sea spray, which is surprising because there are many local and global sources related to mineral dust compared to the single source for sea salt.

The highest COD values for the factors furnace slacks, road wear, construction and mineral dust were found between AD, LE and WZ. This suggests the contribution at these sites is a combination of several local sources with a location-specific source contribution ratio (*e.g.* WZ: primarily furnace slacks; LE: primarily building/construction). The importance of local source contributions was also observed for black carbon and ultrafine particles measured at the same sites.[10] The low COD values for the factors furnace slacks, road wear, construction and mineral dust between AP and LL suggests that the associated sources in these two areas may still be local but similar in composition.

4.4 Wind-directional and Trajectory Analysis of the Source Profiles

Figure 6 shows CPF plots for the contributions of some example source profiles and sites. In these plots the largest peaks points towards the wind sector responsible for the highest contribution at a site. A high contribution of nitrate-rich SA was associated with wind coming from the northeast-east at all the sites, as illustrated for AP (Figure 6a). The contributions of sulfate-rich SA showed a similar pattern as for the nitrate-rich profile (not shown). In general, eastern winds bring in more air pollution compared to western winds. The contributions of sources from Eastern Europe are accumulated leading to higher PM concentrations compared to the relatively cleaner air from the west travelling primarily over the ocean.

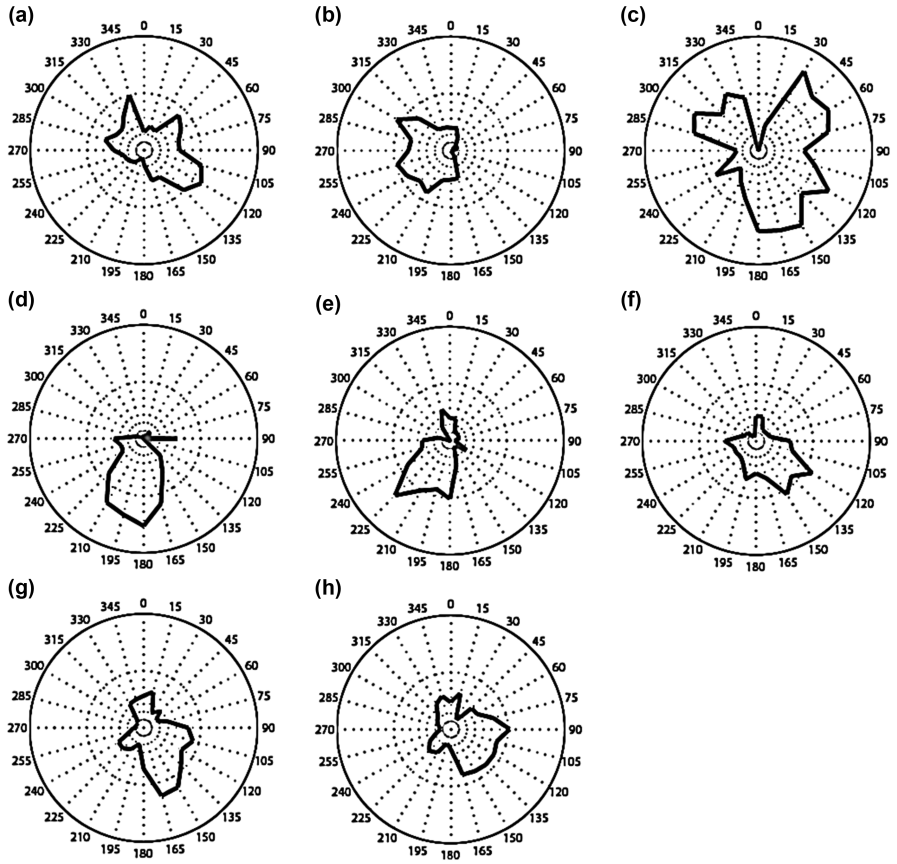

Figure 6 Examples of conditional probability function plots of the contributions of the PM_{10} source profile (a) nitrate-rich secondary aerosol at AP, (b) sea spray at AD, (c) biomass burning at LL, (d) steel industry at WZ, (e) residual oil combustion at WZ, (f) mineral dust at LE, (g) traffic emissions at AP and (h) brake wear at AP.

For the sea spray and aged sea spray profiles, the four sites on the European mainland had the highest contributions from the west, corresponding with the location of the North Sea. This is shown for sea spray at AD (Figure 6b). The highest contributions for (aged) sea spray were found at WZ (Table 3), which is the site closest to the North Sea. For the UK site LE, the highest contribution of sea salt came from the southwest, while the aged sea spray profile seemed to behave like an area source with equal contributions from every direction (not shown).

Figure 7 shows the CPF plots of the Cr profile at AD, AP, LE and LL in combination with a selection of the largest registered sources of Cr in NW Europe (data from 2013). Note that a scaling is used in the CPF plots, so that the size of the peaks in the plots does not correspond with the actual concentrations from a particular wind sector. As mentioned, the highest

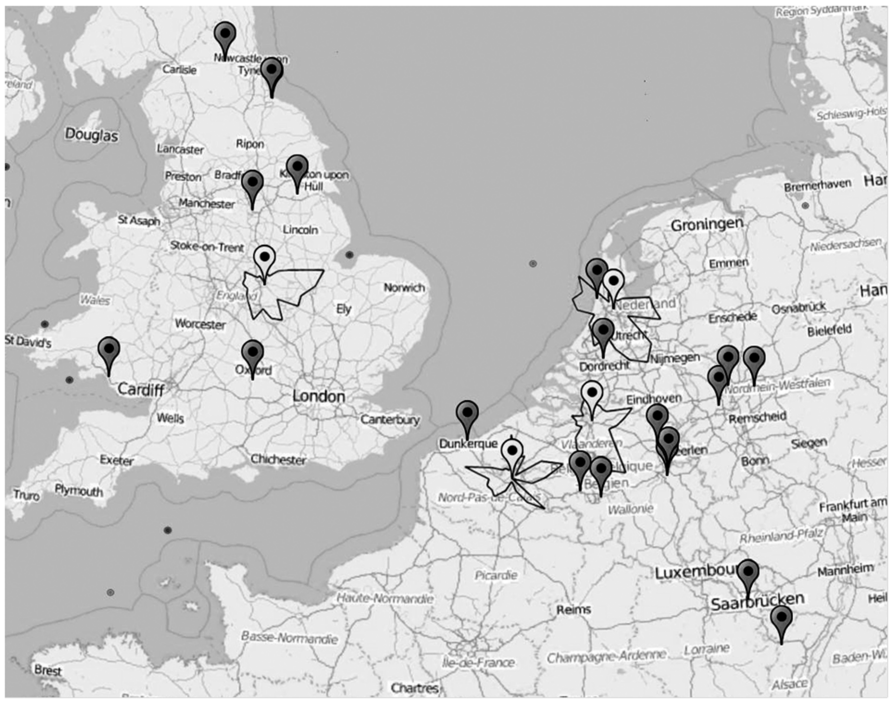

Figure 7 Conditional probability function plots of the contributions of the metal industry/chemical processing (Cr) profile at four sites, indicated by the white symbols (AD, AP, LE and LL). Grey symbols indicate some of the largest registered Cr sources according to the European Pollutant Release and Transfer Register (E-PRTR, http://prtr.ec.europa.eu, data of 2013).

concentrations of the metal industry/chemical processing (Cr) profile were found at AD, AP and WZ (Table 3). The largest contribution of the metal industry/chemical processing (Cr) profile was found on 3 March 2014 at AD. The back-trajectories for this day indicate that the air picks up several emissions from Cr sources located south of AD (Figure 8). The impact of Cr sources at LE seems to be coming primarily from the European mainland (Figure 7).

For biomass burning, the highest concentrations at AD and WZ during the monitoring period were found from the east (not shown). This is related to the Easter bonfires on 20 April 2014 in large parts in the east of Netherlands and Germany, as indicated by the HYSPLIT backward trajectories shown for AD (Figure 9). The biomass burning profile had the highest concentrations at LL (Table 3) and showed contributions from several wind directions (Figure 6c). This indicates that multiple sources associated with biomass burning are affecting the receptor site LL.

The steel industry (Fe) profile was a local source associated with WZ only (Table 3). The highest contributions for steel industry (Fe) were found from the south of WZ (Figure 6d), coinciding with the location of a major steel

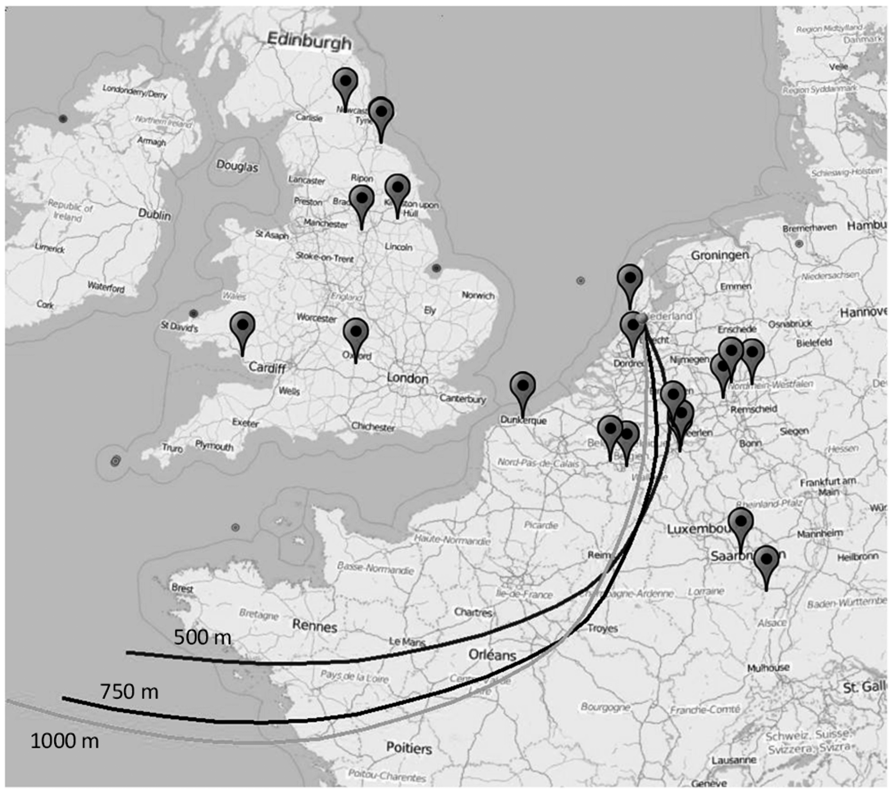

Figure 8 HYSPLIT model analysis with backward trajectories ending at site AD on 3 March 2014, 23:00 UTC. Grey symbols: see Figure 7. The three lines have different starting heights above ground level (500, 750 and 1000 m).

industry in the IJmond industrial area. For the source profile furnace slacks, road wear, construction and mineral dust, the major contribution at WZ was also coming from the south. This finding corresponds well with the assumption that the concentrations in this profile were partly contributed by furnace slacks, which are a by-product of steel manufacturing. The plots for the residual oil combustion profile at AD, AP and WZ point towards shipping emission sources, *e.g.* for WZ there was a strong influence of the port of IJmuiden SW of the site (Figure 6e).

The mineral dust profile showed the highest contributions from the east for the sites on the European mainland and from the S-SE for LE (Figure 6f). For the traffic emissions profile, the majority of the concentrations were contributed by local sources. Although the wind data used in this study are not necessarily representative for the local situation at the aerosol sampling sites, the traffic emission contributions at *e.g.* AP point towards the location of a traffic junction near the site (Figure 6g). The same holds true for the brake wear profile points at AP (Figure 6h).

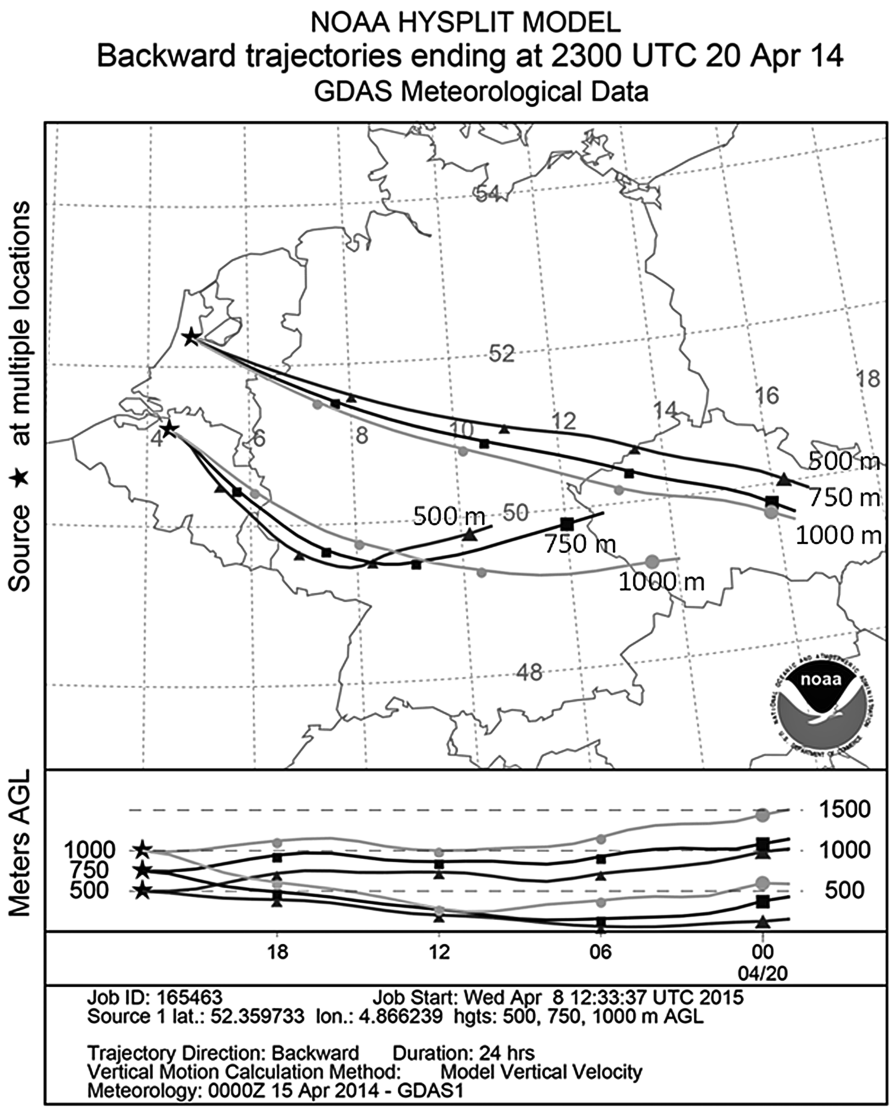

Figure 9 HYSPLIT model analysis with backward trajectories ending at sites AP and AD on 20 April 2014, 23:00 UTC. Lines: see Figure 8.

4.5 Source Profiles on Days Exceeding the Daily Limit Value

Using the calculated PMF source profiles, the dominant source contributions were evaluated for days with known PM_{10} composition on which the concentrations exceeded 50 μg m^{-3} ($n = 8$ for AD, 18 for AP, 7 for LE, 10 for LL and 11 for WZ). The calculated source with the highest contribution was found to be nitrate-rich SA at all sites, as illustrated for AP and WZ (Figure 10). The contribution of this source during exceedance days was on

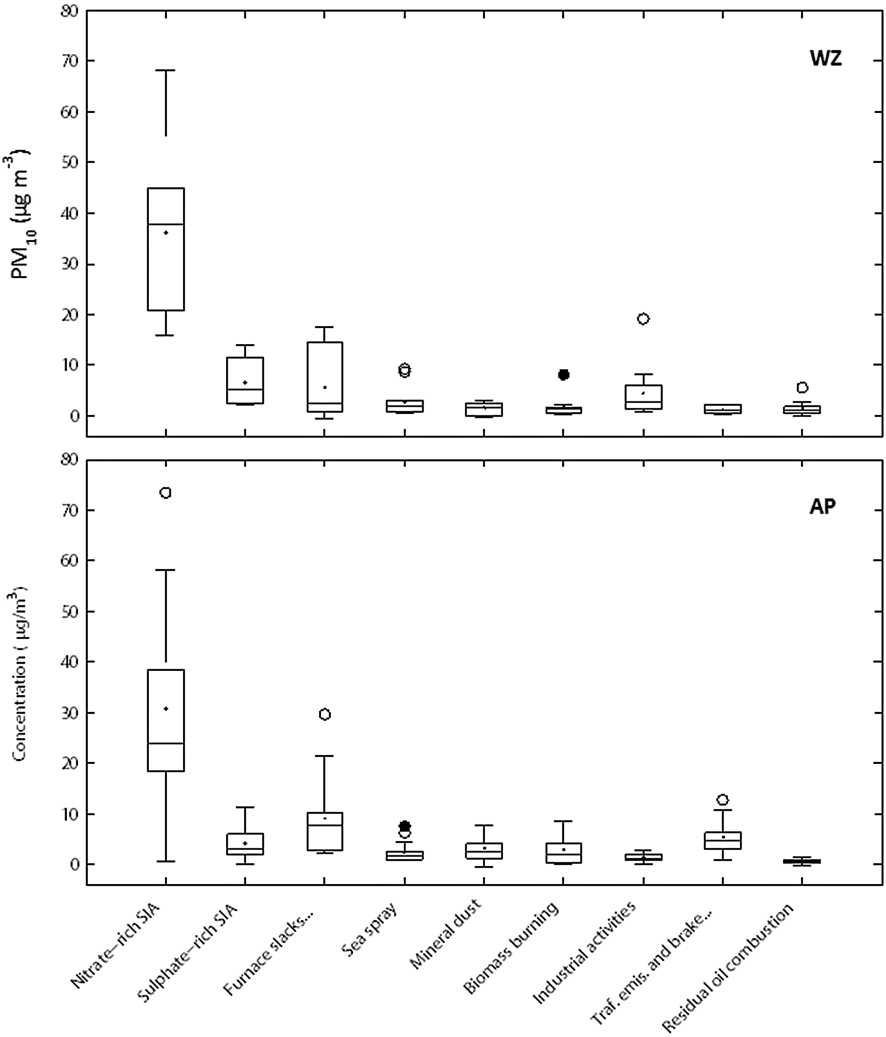

Figure 10 Apportioned PM_{10} concentration per aggregated source profile on days with analysed PM_{10} composition on which PM_{10} exceeded 50 µg m^{-3} at sites WZ and AP.

average 35 ± 18 µg m^{-3} for all sites. The highest mean contribution during exceedance days was found at AD (43 ± 13 µg m^{-3}) and the lowest at LE (32 ± 12 µg m^{-3}). This is in line with other studies in *e.g.* Flanders[52] and the Netherlands.[34] The majority of exceedance days occurred during spring. This is likely related to increased emissions of NH_3 when manure is spread on agricultural lands, and the subsequent increase in the formation of NH_4NO_3. There were also exceedance days with relatively low contributions of nitrate-rich SA, in the winter period when NH_3 emissions are lower.[50] This can probably be attributed to meteorological conditions that are

unfavourable to air dispersion. In winter, a lower inversion layer is generally observed, resulting in a lower mixing height and higher PM concentrations.

Sulfate-rich SA remained fairly constant during exceedance days with a mean contribution of 6 ± 4 μg m^{-3} for all sites. This suggests that SO_2 is not driving increased PM levels, in contrast to NH_3.[50] For AP and LL the second most important source during exceedances days was the furnace slacks, road wear and construction source, with contributions of 9 ± 7 μg m^{-3} (AP) and 12 ± 14 μg m^{-3} (LL). The contribution to PM_{10} of the combined sea salt profiles was fairly constant on all sites with an average of 3 ± 2 μg m^{-3}. The contribution of other sources, such as mineral dust, biomass burning, industrial activities, traffic and residual oil combustion, was small and fairly constant. For some exceedance days, however, for example at WZ, local sources had a meaningful impact on PM_{10}.

4.6 Estimated Uncertainty of the PMF Analysis

The bootstrap (BS) method showed that some high elemental concentrations (*e.g.* Fe and Cr at WZ) critically influenced the bootstrap results. If the peak concentrations for Fe are not present in the bootstrap data set, the steel industry factor is not found and cannot be matched to the base run factor (74% BS mapping). The same phenomenon is observed for Cr (79% mapping). All other factors have approximately 95–100% mapping from the base runs. The displacement of factor elements method (DISP) indicated that there was no significant rotational ambiguity and that the solution was sufficiently robust to be used. The decrease in Q was small ($dQ_{DISP} < 0.1\%$), indicating that a true global minimum of Q was likely found in the base run.[24] Furthermore, no factor swaps were observed in the DISP method, indicating the solution has no or few data errors so that the solution can be considered to be well defined.[25] For the bootstrap enhanced by displacement of factor elements (BS-DISP) method, 71% of the runs were accepted, indicating some uncertainty in the chosen solution. However, the number of swaps can be considered as not fatal to the analysis when positive BS and DISP results as well as clear interpretable factors are found.[26]

The interval ratios of the BS, DISP and BS-DISP methods[25,26] are reported in detail elsewhere.[19] For the key species of both the nitrate-rich and sulfate-rich SA profiles, the interval ratios for the three uncertainty methods were low, indicating a very stable apportionment of NO_3^-, NH_4^+ and SO_4^{2-}. Much higher interval ratios and a higher variation between the ratios of the three methods indicated instability of OC in the sulfate-rich SA. For the profile furnace slacks, road wear, construction and mineral dust, Ca and Ca^{2+} seemed the main key species. Other key species in this factor such as Al and Ti had higher interval ratios, probably owing to the large amount of missing data for these species. The key species for both fresh (Na^+, Mg^{2+} and Cl^-) and aged sea salt (Na^+, Mg^{2+}) showed low interval ratios for all three error estimation methods, indicating that the apportionment of this profile is very stable. For K^+ and OC in the mineral dust profile, the higher interval ratios

for BS-DISP were high compared to the other methods, indicating that the apportionment of these species shows instability. The apportionment of the biomass burning profile, with low interval ratios for the key species levoglucosan, galactosan and mannosan, was very stable. For the distinguished traffic-related factors, the primary traffic emissions profile with key species EC, NO and NO_2, is the most stable solution. For the brake wear profile, Cu appeared to be the main key species, whereas other key species such as Ba, Mo and Sb had higher ratios. The difference between the interval ratios of the different methods indicates that the apportionment of the brake wear profile was not completely stable. This can be explained by the data pooling for sites with differences in the amount and composition of brake wear contributions, *e.g.* owing to differences in traffic intensities, road infrastructure (*e.g.* traffic lights) and the presence of other sources (*e.g.* train shunting facility). Some instability issues were also found for the industry factors (Cr, Fe, As and Cd) and the residual oil combustion factor (Ni, V). In this study the contributions from the industry factors as well as the residual oil combustion differ among the receptor sites and have different local impacts. We established earlier that steel industry has a major impact at WZ whereas higher contributions from residual oil combustion can be seen at sites impacted by shipping emissions.

5 Conclusions

The aim of this study was to identify and quantify the most relevant sources of PM_{10} in NW Europe using positive matrix factorization (PMF). Based on PM_{10} sampling at four urban background sites and one industrial site, an overview of global sources impacting the studied sites was established. A solution with 13 factor profiles was selected, which could be aggregated to eight groups: secondary aerosol; furnace slacks, road wear and construction; sea spray; mineral dust; biomass burning; industrial activities; traffic emissions and brake wear; and residual oil combustion. The largest part of PM_{10} (40–48%) was explained by nitrate-rich (27–37%) and sulfate-rich (9–13%) secondary aerosol. The second-most important source profiles were related to sea spray and aged sea spray (11–21%). These findings correspond with previous source apportionment studies in the Netherlands.[22,35] The source profile furnace slacks, road wear and construction was on average the third most important, but there was more variation between the receptor sites. In addition, clear traffic and biomass burning source profiles were found. Decreasing the emissions of precursor gases of secondary inorganic aerosol, and particularly NH_3 and NO_x, can contribute to decreasing the ambient PM_{10} concentrations in the study region.

The relationship between the measured and apportioned PM_{10} mass per site was good ($R^2 > 0.94$), except for the site in Leicester ($R^2 = 0.81$), suggesting that the current suite of profiles and corresponding contributions are not an optimum match for this site. Combining the data from sites still gives information about local sources, provided the contribution is strong

enough (*e.g.* traffic emissions near the urban sites, the steel industry near the site in Wijk aan Zee). The results of the error estimations for the 13-factor solution show that the apportionment of some factors (secondary aerosol, sea salt, biomass burning and traffic emissions) is stable across the five receptor sites. Other profiles (*e.g.* industrial, brake wear) are subjected to some instability in the PMF analysis, indicating that either the error uncertainties are not accurate and/or the contributions of these factor profiles vary per site or over time. It is recommended to complement this pooled PMF analysis with site-specific source apportionment modelling.

Acknowledgements

This study was carried out in the framework of the Joint Air Quality Initiative (Joaquin), an EU cooperation project supported by the INTERREG IVB North West Europe programme (http://www.nweurope.eu). We thank all the persons who contributed to the PM_{10} sampling and chemical analyses.

References

1. *Air quality in Europe – 2014 report*. EEA Report No 5/2014, European Environment Agency, Luxemburg, 2014.
2. *Air quality guidelines. Global update 2005. Particulate matter, ozone, nitrogen dioxide and sulfur dioxide*. World Health Organization, Regional Office for Europe, Copenhagen, 2006.
3. F. J. Kelly and J. C. Fussell, *Atmos. Environ.*, 2012, **60**, 504.
4. *Directive 2008/50/EC of the European Parliament and of the Council of 21 May 2008 on ambient air quality and cleaner air for Europe*. *Off. J. Eur. Union*, 11.6.2008, 1–44.
5. C. A. Belis, B. R. Larsen, F. Amato, I. El Haddad, O. Favez, R. M. Harrison, P. K. Hopke, S. Nava, P. Paatero, A. Prevot, U. Quass, R. Vecchi and M. Viana. *European guide on air pollution source apportionment with receptor models*, European Commission, Joint Research Centre, Institute for Environment and Sustainability, report EUR 26080 EN. Publications Office of the European Union, Luxembourg, 2014.
6. P. K. Hopke, *A Guide to Positive Matrix Factorization*, Available at: http://people.clarkson.edu/~hopkepk/PMF-Guidance.htm, 2003.
7. J. Vercauteren, C. Matheeussen, E. Wauters, E. Roekens, R. van Grieken, A. Krata, Y. Makarovska, W. Maenhaut, X. Chi and B. Geypens, *Atmos. Environ.*, 2011, **45**, 108.
8. E. P. Weijers, M. Schaap, L. Nguyen, J. Matthijsen, H. A. C. Denier van der Gon, H. M. ten Brink and R. Hoogerbrugge, *Atmos. Chem. Phys.*, 2011, **11**, 2281.
9. Air Quality Expert Group, *Fine Particulate Matter ($PM_{2.5}$) in the United Kingdom*, Department for Environment, Food and Rural Affairs, London, UK, 2012. Available at https://www.gov.uk/government/uploads/system/

uploads/attachment_data/file/69635/pb13837-aqeg-fine-particle-matter-20121220.pdf.
10. *Monitoring of ultrafine particles and black carbon. Joint Air Quality Initiative (Joaquin), work package 1 action 1 and 3*. Flanders Environment Agency, Aalst, 2015. Available at http://joaquin.eu.
11. Nationaal Samenwerkingsprogramma Luchtkwaliteit (NSL), The Netherlands. Available at: https://www.nsl-monitoring.nl/viewer.
12. Department for Transport, London, UK. Available at http://www.dft.gov.uk/traffic-counts.
13. *Intra-urban variability of ultrafine particles in Antwerp (February and October 2013)*. Flanders Environment Agency, Erembodegem, 2014. Available at http://www.vmm.be.
14. EN 14907. *Ambient air quality – Standard gravimetric measurement method for the determination of the $PM_{2.5}$ mass fraction of suspended particulate matter*. European Committee for Standardization, Brussels, 2005.
15. R. L. Cordell, I. R. White and P. S. Monks, *Anal. Bioanal. Chem.*, 2014, **406**, 5283.
16. CEN/TR 16243. *Ambient air - Guide for the measurement of elemental carbon (EC) and organic carbon (OC) deposited on filters*. European Committee for Standardization, Brussels, 2011.
17. CEN/TR 16269. *Ambient air - Guide for the measurement of anions and cations in $PM_{2.5}$*. European Committee for Standardization, Brussels, 2011.
18. A. Yang, A. Jedynska, B. Hellack, I. Kooter, G. Hoek, B. Brunekreef, T. A. J. Kuhlbusch, F. R. Cassee and N. A. H. Janssen, *Atmos. Environ.*, 2014, **83**, 35.
19. *Composition and source apportionment of PM_{10}. Joint Air Quality Initiative (Joaquin), work package 1 action 1 and 2*. Flanders Environment Agency, Aalst, 2015. Available at http://joaquin.eu.
20. D. B. Rubin, *Biometrika*, 1976, **63**, 581.
21. P. K. Hopke, *Chemom. Intell. Lab. Syst.*, 1991, **10**, 21.
22. D. Mooibroek, M. Schaap, E. P. Weijers and R. Hoogerbrugge, *Atmos. Environ.*, 2011, **45**, 4180.
23. G. Norris, R. Vedantham, K. Wade, S. Brown, J. Prouty, C. Foley, *EPA Positive Matrix Factorization (PMF) 3.0 Fundamentals and User Guide*, U.S. Environmental Protection Agency, Washington, DC, 2008, EPA 600/R-08/108.
24. G. Norris, R. Duvall, S. Brown, S. Bai, *EPA Positive Matrix Factorization (PMF) 5.0 Fundamentals and User Guide*, U.S. Environmental Protection Agency, Washington, DC, 2014, EPA/600/R-14/108.
25. P. Paatero, S. Eberly, S. G. Brown and G. A. Norris, *Atmos. Meas. Tech.*, 2014, **7**, 781.
26. S. G. Brown, S. Eberly, P. Paatero and G. A. Norris, *Sci. Total Environ.*, 2015, **518–519**, 626.
27. P. Paatero, P. K. Hopke, X. H. Song and Z. Ramadan, *Chemom. Intell. Lab. Syst.*, 2002, **60**, 253.

28. P. Paatero, *User's Guide for Positive Matrix Factorization Programs PMF2 and PMF3, Part 2: Reference, Tutorial*, 2000.
29. E. Kim, P. K. Hopke, J. P. Pinto and W. E. Wilson, *Environ. Sci. Technol.*, 2005, **39**, 4172.
30. E. Kim and P. K. Hopke, *Atmos. Environ.*, 2004, **38**, 4667.
31. E. Kim, P. P. Hopke and E. S. Edgerton, *J. Air Waste Manage. Assoc.*, 2003, **53**, 731.
32. R. R. Draxler and G. D. Hess, *Austr. Meteorol. Mag.*, 1998, **47**, 295.
33. N. M. Donahue, A. L. Robinson and S. N. Pandis, *Atmos. Environ.*, 2009, **43**, 94.
34. M. Schaap, E. P. Weijers, D. Mooibroek, L. Nguyen, *Composition and origin of particulate matter in the Netherlands*. Bilthoven, the Netherlands, PBL report 500099007, 2010.
35. D. Mooibroek, E. van der Swaluw, R. Hoogerbrugge. *A reanalysis of the BOP dataset: Source apportionment and mineral dust*. National Institute for Public Health and the Environment, Bilhtoven, RIVM Rapport 680356001, 2012.
36. S. H. Cadle, P. A. Mulawa, J. Ball, C. Donase, A. Weibel, J. C. Sagebiel, K. T. Knapp and R. Snow, *Environ. Sci. Technol.*, 1997, **31**, 3405.
37. D. S. Lee and J. M. Pacyna, *Atmos. Environ.*, 1999, **33**, 1687.
38. M. J. Kleeman, J. J. Schauer and G. R. Cass, *Environ. Sci. Technol.*, 2000, **34**, 1132.
39. M. Valius, *Characteristics and sources of fine particulate matter in urban air*, PhD thesis, University of Kuopio, Finland, 2005.
40. H. Beuck, U. Quass, O. Klemm and T. A. J. Kuhlbusch, *Atmos. Environ.*, 2011, **45**, 5813.
41. A. Waked, O. Favez, L. Y. Alleman, C. Piot, J.-E. Petit, T. Delaunay, E. Verlinden, B. Golly, J.-L. Besombes, J.-L. Jaffrezo and E. Leoz-Garziandia, *Atmos. Chem. Phys.*, 2014, **14**, 3325.
42. J. G. Watson and J. C. Chow, *Sci. Total Environ.*, 2001, **276**, 33.
43. N. J. Kuhn, *Earth Surf. Processes Landforms*, 2007, **32**, 794.
44. V. Bernardoni, R. Vecchi, G. Valli, A. Piazzalunga and P. Fermo, *Sci. Total Environ.*, 2011, **409**, 4788.
45. A. J. Fernández-Espinosa and M. Ternero-Rodríguez, *Anal. Bioanal. Chem.*, 2004, **379**, 684.
46. *Geochemical Atlas of Europe. Part 1: Background Information, Methodology and Maps*, ed. R. Salminen, M. J. Batista, M. Bidovec and A. Demetriades, ISBN 951-690-921-3, p. 525 (printed) & 951-690-913-2 (electronic version), 2005.
47. H. A. C. Denier van der Gon, J. H. J. Hulskotte, A. J. H. Visschedijk and M. Schaap, *Atmos. Environ.*, 2007, **41**, 8697.
48. Olmez, A. E. Sheffield, G. E. Gordon, J. E. Houck, L. C. Pritchett, J. A. Cooper, T. G. Dzubay and R. L. Bennett, *J. Air Waste Manage. Assoc.*, 1988, **38**, 1392.
49. M. Pandolfi, Y. Gonzalez-Castanedo, A. Alastuey, J. D. de la Rosa, E. Mantilla, A. S. de la Campa, X. Querol, J. Pey, F. Amato and T. Moreno, *Environ. Sci. Pollut. Res. Int.*, 2011, **18**, 260.

50. A. Backes, A. Aulinger, J. Bieser, V. Matthias and M. Quante, *Atmos. Environ.*, 2015, **126**, 153.
51. X. Querol, A. Alastuey, M. M. Viana, S. Rodriguez, B. Artiñano, P. Salvador, S. Garcia do Santos, R. Fernandez Patier, C. R. Ruiz, J. de la Rosa, A. Sanchez de la Campa, M. Menendez and J. I. Gil, *J. Aerosol Sci.*, 2004, **35**, 1151.
52. *Chemkar PM_{10} – Second city campaign: Chemical characterisation of particulate matter in Mechelen, Leuven, Kortrijk, Hasselt en Aalst, 2013-2014* [in Dutch]. Flanders Environment Agency, Aalst, 2015. Available at http://www.vmm.be.
53. E. Kim and P. K. Hopke, *Atmos. Environ.*, 2008, **42**, 6047.

ECN
Westerduinweg 3
1755 LE Petten

Postbus 1
1755 ZG Petten

T 088 515 4949
F 088 515 8338
info@ecn.nl
www.ecn.nl